POLITECNICO DI TORINO
Repository ISTITUZIONALE

Assessment of robustness of reinforced concrete frame structures with masonry infill walls

(Article begins on next page)

11 May 2024

ASSESSMENT OF ROBUSTNESS OF REINFORCED CONCRETE FRAME STRUCTURES WITH MASONRY INFILL WALLS

F. Di Trapani[1], L. Giordano[1], G. Mancini[1] and M. Malavisi[1]

[1] Dipartimento di Ingegneria Strutturale, Edile e Geotecnica, Politecnico di Torino, Torino, Italy
{fabio.ditrapani,luca.giordano,giuseppe.mancini,marzia.malavisi}@polito.it

Abstract

Robustness of frame structures is fundamental to limit progressive collapse of buildings in case of accidental loss of columns. The interest in robustness assessment is growing in recent years especially for reinforced concrete structures, which are commonly analyzed considering the bare frame configuration. This paper presents a numerical study highlighting the influence of masonry infill walls on the robustness of reinforced concrete frame structures. The main geometrical and mechanical parameters identifying an infilled frame (aspect ratio, seismic detailing, lateral constrain degree) are investigated by performing parametric pushdown tests on reference two-bay frames extracted from different types of buildings. The tests are carried out by using a detailed finite element model of the infilled frame. Results show significantly different responses from bare and infilled frames in terms of resistance and displacement capacity under the different conditions tested. In a relevant a number of cases infills have shown to be fundamental to limit or avoid multiple collapses.

Keywords: Robustness, Infilled frames, Reinforced concrete, Masonry, Pushdown, Catenary

1 INTRODUCTION

In the last years, the interest in structural robustness is rapidly increasing within the scientific community and in practice engineering. For civil structures having residential, commercial or public use, the limitation damage propagation in consequence of the accidental loss of a primary structural element, such as a column, is fundamental to prevent public safety and reduce economic losses. Robustness based design of buildings addresses solutions to avoid that damage suffered by a structure, due to an accidental event, would not be disproportionate with respect to the cause that has caused it, as several times occurred in the past (Fig. 1). In frame structures, the loss of a perimetral column due to impacts, explosions or advanced material degradation may result into serious consequences for the whole building which depend

on several conditions such as the location of the collapsed element, the shape of the bays, the type of frame elements and the arrangement of the reinforcement.
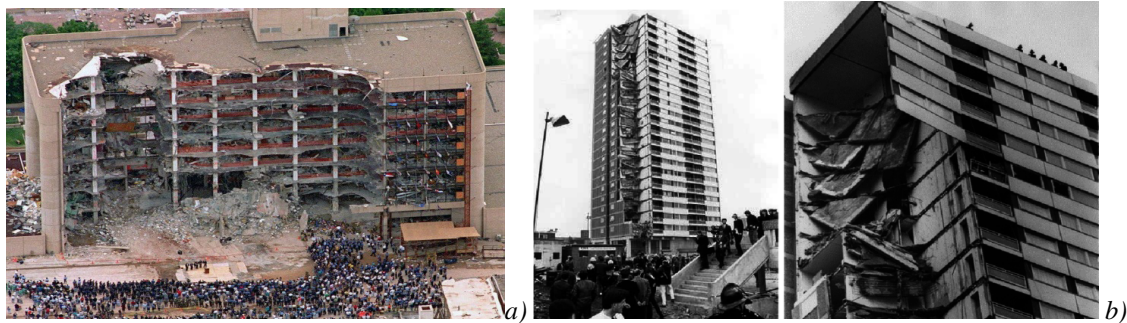

Figure 1: Examples of progressive collapses: a) Alfred P. Murrah Federal Building, Oklahoma City, 1995; b) Ronan Point Building, London, 1968.

For reinforced concrete bare frame structures, the possibility of avoiding or limiting multiple collapses as a consequence of a column loss, depends on the capacity of the connected beams to switch from the first flexural and arching resistant mechanism, to a catenary tensile mechanism under large displacements regime. In the recent past, several studies have addressed progressive-collapse response of frame structures. Among these [1,2] formulated a simplified method for the determination of dynamic load-displacement demand, through a pseudo-static procedure. Experimental tests on reduced scale and real RC structures have been also carried out [3,4]. Further experimental investigations, accompanied by numerical studies, were provided in [5-9]. The principal findings of these studies report that ductility of beam end cross-sections has an important role on the possible activation of the catenary mechanism, but many other factors condition the response as for example the horizontal constraint degree the actual capacity of elongation rebars and the height to length ratio of beams.

It should be evidenced that the aforementioned studies did not consider the influence of infills on the progressive collapse mechanism, although infill-frame interaction effects are well known and have been widely documented for the case of lateral forces by a number of experimental studies and numerical investigations [10-19]. Only in the last few years the influence of masonry infills on the progressive collapse response has known the first numerical studies regarding masonry infilled steel frames [20, 21], and two experimental investigations on infilled RC structures [22, 23]. These studies revealed the significant modification of the resisting mechanisms due to the noticeable strength increase and the alternative load pattern which develops. As a consequence of this, sufficient reliability [24-35] in estimating progressive collapse response of infilled frames (IF) cannot be achieved without explicitly considering frame-infill interaction. Further the role played by different geometrical and mechanical parameters remains unknown even in terms of dynamic load amplification and safety levels.

Based on this background, the paper presents a study investigating parameters influencing the robustness of RC structures with masonry infills in terms of resisting capacity and dynamic amplification of the response in comparison with bare frames. Three reference case study building structures have been designed with and without considering seismic load and detailing. The pushdown response is obtained from refined finite element models of 2D substructures. Numerical tests regarded a significant number of parameters such as lateral constraint degree, aspect ratio of the infilled frame, seismic detailing). Finally, possible single strut and multiple strut modelling configurations are tested and compared.

2 ANALYISIS PROGRAM AND STRUCTURAL MODELS DEFINITION

The case study of a five-storey RC frame residential building is considered as reference. It is supposed the accidental loss of a column placed at the center of a perimeter frame. The building structures have been designed hypothesizing two different arrangements of central bays, one with short spans and beam length (l_b) column length (h_c) aspect ratio l_b/h_c=1 (Building A) (Fig. 2a), the other having long spans and l_b/h_c=2 (Fig. 2b) (Building B). Buildings A and B have deep beams (30x50 cm). Design strength of concrete (f_c) and steel (f_y) are 25 MPa and 450 MPa respectively. Design loads of inter-floor slabs are G_{1k}=3.20 kN/m, G_{2k}=3.80 kN/m, Q_{k1}=2.00 kN/m. Buildings A and B have been designed with and without considering seismic loads, seismic detailing and capacity design. In the first case the site hazard of Palermo (Italy) is selected in combination with a Type A (hard) soil, a reference life (V_N) of 50 years, and a return period (T_R) of 475 years. For the second case buildings A and B are designed considering only vertical loads and disregarding seismic detailing rules. Reinforcement detail of the extracted sub-frames is shown in Figs. 3-5. The influence of the horizontal constraint degree, provided by the adjacent frames, on the progressive collapse response is also investigated. Pushdown tests on the sub-frames are then carried out in the two boundary cases of: *i*) full lateral constraint; *ii*) no lateral constraint.

Masonry infill walls are supposed to be the same typology as the one tested by [12], arranged with clay hollow bricks. Experimental mechanical parameters are shown in Table 1, and are referred to direction 1 (parallel to mortar joints) and direction 2 (orthogonal to mortar joints). For the current case, the units are supposed being 30 cm thick, 32 cm long and 26 cm high. Summarizing, investigated parameters are the aspect ratio of the frames (l_b/l_c), the aspect ratio of the beams (h_b/t_b of the beam), the type of reinforcement design (seismic / non-seismic), the effectiveness of the lateral constraints (rigid or free). For every case bare frame and infilled frame conditions are analized.
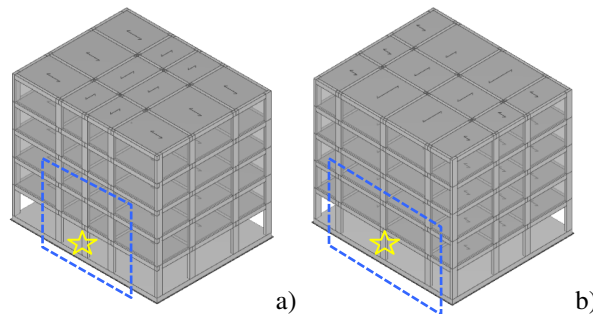

Figure 2: 3D view of case study buildings and extracted sub-frames: a) Building A; b) Building B; c) Building C; d) Building D.
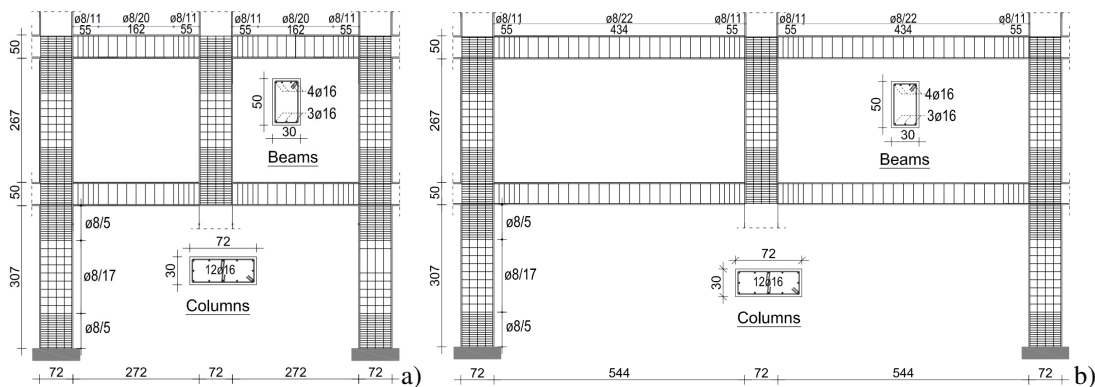

Figure 3: Sub-frames with seismic design extracted from: a) building A; b) building B.
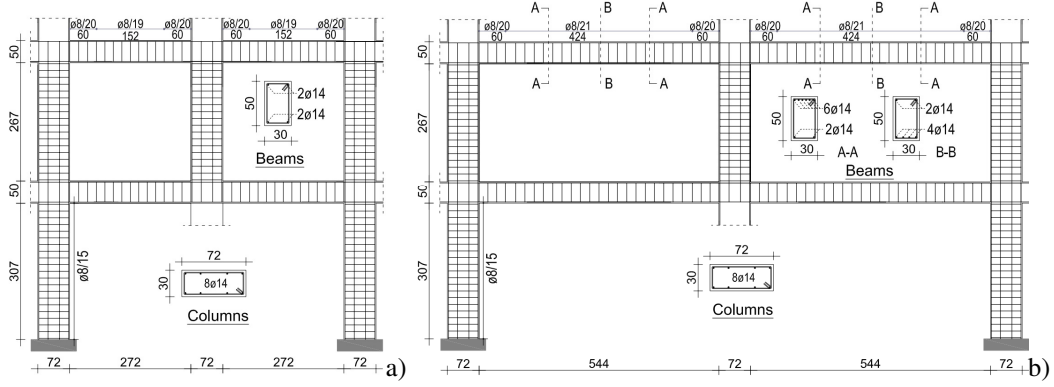
Figure 4: Sub-frames without seismic design extracted from: a) building A; b) building B.

f_{m1} (MPa)	f_{m2} (MPa)	f_{vm} (MPa)	E_1 (MPa)	E_2 (MPa)	G (MPa)
4.18	8.66	1.07	5032	6401	2547

Table 1: Mechanical parameters of masonry constituting infills [12].

3 DEFINITION OF THE FE MODEL AND TEST MODALITIES

3.1 The FE model

The extracted sub-frames are reproduced with a refined nonlinear FE model realized in ATENA 2D [34]. The assembly of the model is depicted in Fig. 6. Concrete element portions and masonry blocks are modeled by using CCIsoQuad nonlinear finite elements [36]. The constitutive model governing the response of concrete elements and masonry units (SBeta material) is defined by a uniaxial stress-strain concrete-type law that is associated with a biaxial domain regulating the failure surface. Compressive strength of concrete elements is assigned to the different element portions taking into account the actual confinement exerted by transverse reinforcement. Nominal concrete mechanical parameters are reported in Table 2. As for the masonry units parameters are initially taken from experimental values reported in Table 1, however, in order to account for the anisotropic behaviour of masonry, conventional compressive strength $\widetilde{f}_m$ and elastic modulus $\widetilde{E}_m$ are obtained by averaging experimental values along the two orthogonal directions [35] while shear strength (f_{vm}) is the same as that experimentally detected from the shear tests. Mechanical parameters used for masonry units and unconfined concrete are summarized in Table 2. Frictional response of mortar joints is simulated by using interface elements between masonry units and between masonry units and concrete. The 2D interfaces are governed a Mohr-Coulomb failure domain which depends on friction coefficient (μ) and cohesion (c). Interface response depends also on tangential and normal stiffness moduli K_{tt} and K_{nn} assumed for the interfaces. Longitudinal reinforcement is accounted by using "embedded rebar" elements with a uniaxial elasto-plastic strain hardening constitutive model with yield stress f_y=450 MPa, ultimate stress f_t=540 MPa and ultimate deformation ε_{su}=12%. Transverse reinforcement is considered within the by means of the smeared reinforcement material, which uniformly spreads shear reinforcement over the mesh of macro-elements. For all the elements described above, geometric nonlinearity is considered to allow carrying out large displacements the analysis.
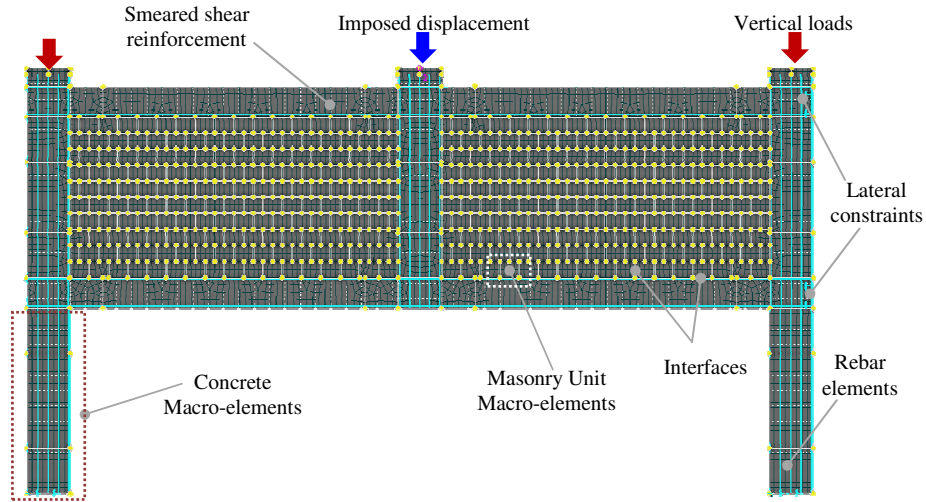
Figure 6: FE model assembly for of an extracted sub-frame.

Unconfined concrete			Masonry unit macro-elements		
f_c (MPa)	f_{ct} (MPa)	E_c (MPa)	$\tilde{f}_m$ (MPa)	$\tilde{E}_m$ (MPa)	f_{vm} (MPa)
25	2	31000	6.42	5716.5	1.07

Table 2: Mechanical parameters of masonry and unconfined concrete macro-elements.

3.2   FE model calibration

Parameters subject to calibration are those associated with the major uncertainty, namely those regarding interface response. In detail these are the normal stiffness modulus (K_{nn}), the tangential stiffness modulus (K_{tt}), the cohesive strength (c), the tensile strength (f_t) and the friction coefficient (μ). Since masonry infills are hollow clay infills of the same type of those tested in [12], it has been reasonably supposed that calibration parameters values should be the same as those obtained in [37] where the same model was used to simulate lateral response of infilled frames experimentally tested in [12]. Interface parameters used are reported in Table 4. It should be said that original experimental tests are lateral force- lateral displacement tests, simulating seismic load conditions, while current load condition refer to vertical loading of the infilled frames. However interface parameters are not significantly affected by loading direction, hence the assumption made of adopting calibration values obtained in [37] for the current models is considered reasonable also in the framework of this study.
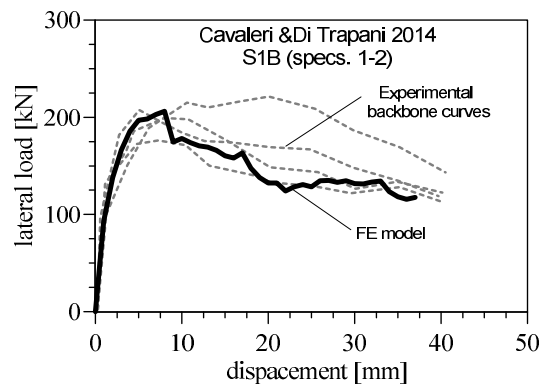

Figure 7: Experimental positive and negative envelopes of specimens S1B [12] and force-displacement response by the FE model after the calibration [37].

Normal stiffness	Tangential stiffness	Tensile strength	Cohesion	Friction coefficient
K_{nn} (MN/m)	K_{tt} (MN/m)	f_t (MPa)	c (MPa)	μ -
4000000	400000	0.4	1.0	0.7

Table 3. Calibrated interface parameters.

3.3 Definition of pushdown tests and capacity / demand assessment

Pushdown tests are conducted in two phases. First, vertical loads are applied at the top of lateral columns (Fig. 6), then, increasing vertical displacement is then imposed to the central column. Vertical displacement and reaction forces are monitored during the tests. The obtained force-displacement curve is the pushdown capacity-curve of the system under the column removal scenario. The static load demand (P_0) for each analyzed system is determined as the rate of axial force previously acting on the removed column (P_s):

$$P_0 = \alpha_{SF} P_s \tag{1}$$

where α_{SF} is a distribution factor obtained as the ratio between the number of floors involved in the sub-frame system ($n_{f,SF}$) and the total number of floors (n_f) as follows:

$$\alpha_{SF} = \frac{n_{f,SF}}{n_f} \tag{2}$$

In the current cases, 2 storey sub-systems are extracted from 5 storey frames, then the distribution facto α_{SF} is 0.4 (2/5). The static load demand to the sub-frames (P_0) is then 260 kN for the systems having $l_b/l_c=1$ ($P_s = 650$ kN) and 480 kN for the systems having $l_b/l_c=2$ ($P_s = 1200$ kN). Under the instantaneous column removal the static load demand is amplified because of the dynamic effect occurring due to the abrupt variation of the equilibrium conditions. The load amplification factor can be estimated through a pseudo static-procedure [1], namely by equating the external work done by gravity loads and the internal work resulting as the area below the pushdown curve. The external work done by gravity loads is the function:

$$W_e(u) = \alpha P_0 u \tag{3}$$

where $\alpha=0.5$ is coefficient considering the fact that loads are distributed over the beams. Eq. (3) represents a straight line passing through 0 and is defined in the interval $[0,u_u]$, where u_u is the ultimate displacement. The internal work is the integral function of the pushdown curve $P(u)$ defined in the interval $[0,u_u]$ obtained as (Fig.:

$$W_i(u) = \int_0^u P(u)du \tag{4}$$

After column removal, the system will achieve a new equilibrium condition if functions $W_i(u)$ and $W_e(u)$ have an interception point in correspondence of the vertical displacement $u=u_d$ (Fig. 8a), representing the dynamic displacement demand to the system. Displacement u_d can be evaluated by setting (Fig. 8a, 8b):

$$W_e(u) - W_i(u) = 0 \tag{5}$$

that is:

$$\alpha P_0 u_d - \int_0^{u_d} P(u)du = 0 \tag{6}$$

After, the dynamic load demand αP_d is evaluated as:

$$\alpha P_d = P(u_d) \tag{7}$$

Therefore the static load amplification factor is:
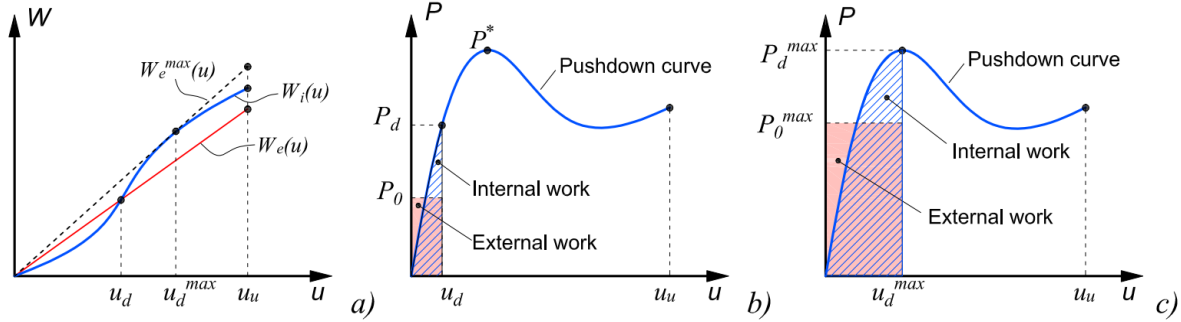
$$\lambda_d = \frac{P_d}{P_0} \tag{8}$$

Figure 8: Framework to evaluate dynamic demand and capacity: a) Internal work and external work functions; b) determination of dynamic load demand; b) determination of maximum capacity.

The capacity / demand ratio of a system can be also expressed as the ratio between the maximum static load to which the sub-frame could be subjected to (P_0^{max}) and the current static load (P_0), that is:

$$\beta_s = \frac{P_0^{max}}{P_0} \tag{9}$$

where P_0^{max} is easily obtained by changing the slope of the line expressed by Eq. (3) in such a way that external work function becomes is tangent to the internal work function (Fig. 8a). In this case Eq. (6) becomes:

$$\alpha P_0^{max} u_d^{max} - \int_0^{u_d^{max}} P(u)\,du = 0 \tag{10}$$

which allows also obtaining maximum dynamic displacement demand u_d^{max} and maximum dynamic load demand αP_d^{max}, which is theoretically coincident with the peak load P^* (Fig. 8c). The capacity/demand ratio β_s can be evaluated even in the case in which a system is not able to achieve a new equilibrium condition. In this case β_s will be lower than 1.

4 INFLUENCE OF ASPECT RATIO, SEISMIC DETAILS AND LATERAL CONSTRAINT DEGREE

4.1 Bare and infilled frames having $l_b/l_c=1$

Pushdown curves of bare and infilled frames having $l_b/l_c=1$ are shown in Figs. 9 and 10. For the case of rigid lateral constraints the pushdown response of bare frames (Fig. 9a) exhibited a resistance peak followed by a rapid loss of resistance. This behaviour is consistent with a significant compressive thrust occurring when arching mechanism develops after the cracking at the beam ends. This justifies the initial increase of flexural capacity of beams. The following bearing capacity loss is related to the achievement of high strain rate of concrete which starts crushing compression. Pushdown tests of infilled frames (Fig. 9b) showed on av-

erage double resistance with respect to bare frames, together with a significant stiffness increase. The increase in strength is strictly related to the modification of the overall resisting mechanism because of the interaction with the infills. This is clear from the comparison of the damage scenarios of the two systems (Figs. 11a-b). The resisting mechanism of bare frame involves 8 plastic hinges at the ends of the beams, as expected for a simple flexural collapse (Fig. 11a). The resisting mechanism of the infilled frame (Fig. 11b) is more complicated. Fist it can be clearly observed the formation of two compression fields characterized by diagonal cracks passing through masonry units. Second, slippage of mortar joints occurs in the central portion of the infill, which is less affected by confinement effect exerted by the frame at the corner regions. The compression fields conveying the diagonal compression stresses on the masonry also influence the local distribution of internal forces of beams. This results in a shifting of the position of plastic hinges (upper beams external hinges and lower beams internal hinges) toward the inner of the beam (at about 35% of the internal length). Steel rebars plastic strain diagrams of bare and infilled frames highlight the position of plastic hinges (Fig. 11a-b). The rapid post-peak strength decay occurs in correspondence of mortar joints sliding.

As for the influence of seismic detailing, it can been observed, that the major strength of seismically designed bare frames with respect to frames with seismic detailing (Fig. 9a) is related to the larger amount of flexural reinforcement arranged to agree code provisions. Conversely, the seismic design of the frame resulted to be not actually relevant in the case of infilled frames if one considers the large strength increment provided by the infills (Fig. 9b).
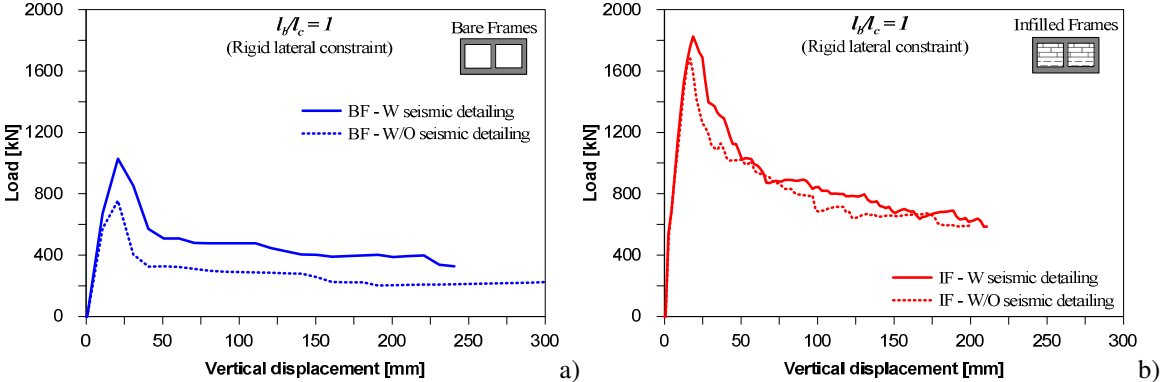

Figure 9: Pushdown curves for specimens with $l_b/l_c=1$ and rigid lateral constraint: a) bare frames with and without seismic detailing; b) infilled frames with and without seismic detailing.
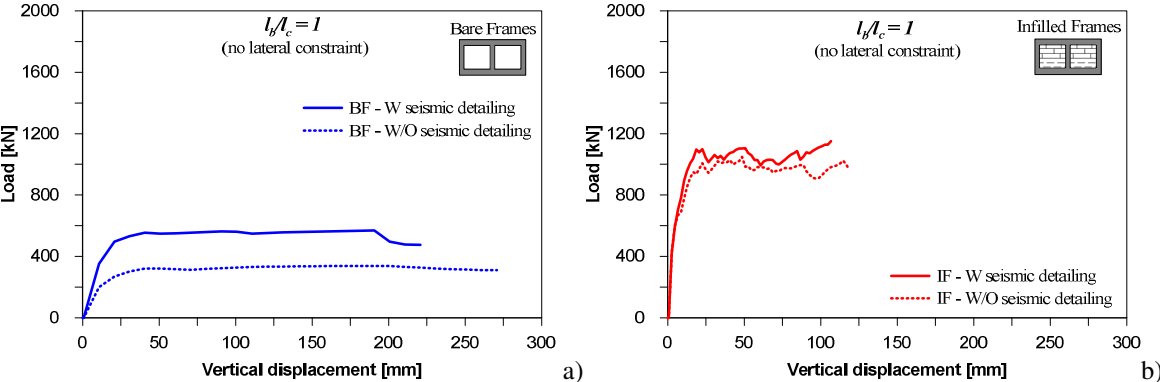

Figure 10: Pushdown curves for specimens with $l_b/l_c=1$ and no lateral constraint: a) bare frames with and without seismic detailing; b) infilled frames with and without seismic detailing.

Some different observations can be done in case of no lateral constraint (Fig. 10), where the larger deformability of the systems has as effect the significant reduction of the compression action on the beams, which is reflected as a reduction of the flexural resistance, ranging between -40% for the infilled frames and -70% for the bare frames. The reduction of the axial force on beams is consistent with the more ductile behaviour observed form the capacity curves. The influence of infills results in a more relevant strength increase action especially for the case of non-seismically designed frames, where strength increment is about 3 times.

It should be finally observed that for all the investigated systems with aspect ratio $l_b/l_c=1$ there was no evidence of activation of the catenary mechanism after the flexural phase. This can be first attributed to the reduced inelastic displacement capacity of the beams, because of the low span length / cross-section height ratio. For the infilled frame cases this is also associated with the overall modification of the resisting mechanism which results in an increase of shear damage to bottom beams at relatively low displacements because of the infills pushing action.
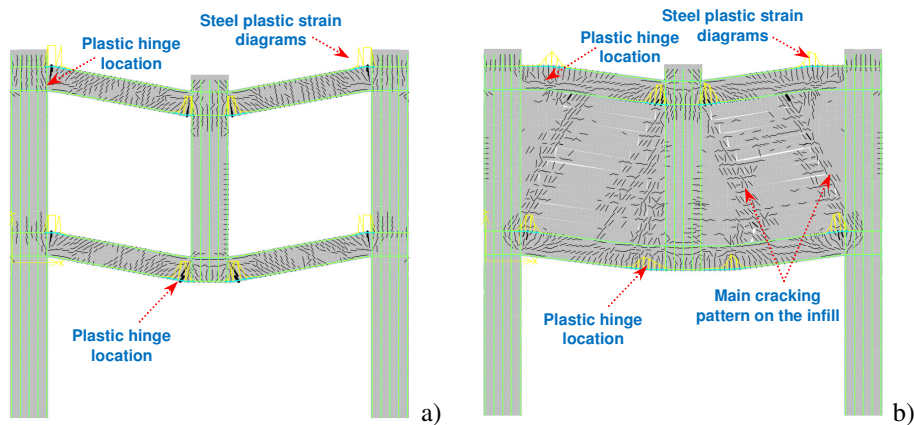

Figure 11: Cracking pattern on the FE model at the end of the pushdown test of specimens with $l_b/l_c=1$ and rigid lateral constrains: a) bare frame; b) infilled frame.

4.2   Bare and infilled frames having $l_b/l_c=2$

Push-down curves of bare and infilled frames with shape factor $l_b/l_c=2$ are shown in Figs. 12 and 13. In the case of rigid lateral constraints (Figs. 12a-b), both the systems exhibit the achievement of a resistance peak followed by a rapid strength decay. Bare frames have shown significantly slight regain of resistance at large deformations due to a moderate activation of the catenary mechanism (Fig. 12a). The final cracking pattern of bare frames test (Fig. 14a) clearly shows the position of plastic hinges at the ends of beams, and the presence of cracks orthogonal to the longitudinal axis of the beams, denoting a uniform tensile stress state.

Infilled frames have shown a resistance increment of about + 50% with respect to bare frames (Fig. 12b). In comparison with square frames, the lower influence of infills to the systems resistance is recognized in this case. This is related the larger deformability of the frame, which can provide effective confinement on a relatively smaller portion of masonry (Fig. 14b).

Slippage and separation of mortar joints, is observed in the central portions of the infills. The migration of the position of plastic hinges toward the center of the beams is more pronounced in this case. The position of plastic hinges is at about 35% of the internal length of the beams. In absence of horizontal constraints, the strength reduction is approximately -40% (Figs. 13a-13b) with respect to the fully restrained case for both bare and infilled frames. The achievement of the maximum load capacity is followed by a post-elastic branch not showing losses or increases in resistance. This highlights on the one hand a more ductile behaviour due

to the reduced axial compression level on beams, and, on the other hand, the inhibition of the catenary mechanism, because of the reduced capacity of the system to support horizontal tension forces.

For all the investigated systems, the presence of seismic detailing resulted to not influence the overall response in a significant way. The small strength increments observable from Figs. 12 and 13 can be entirely associated with the larger amount of longitudinal reinforcement.
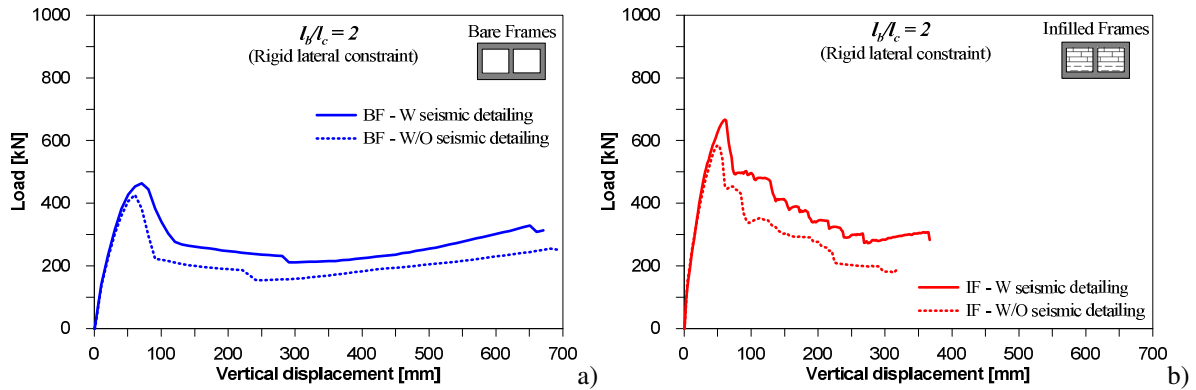

Figure 12: Pushdown curves of specimens with l_b/l_c=2 and rigid lateral constraints: a) bare frames with and without seismic detailing; b) infilled frames with and without seismic detailing.
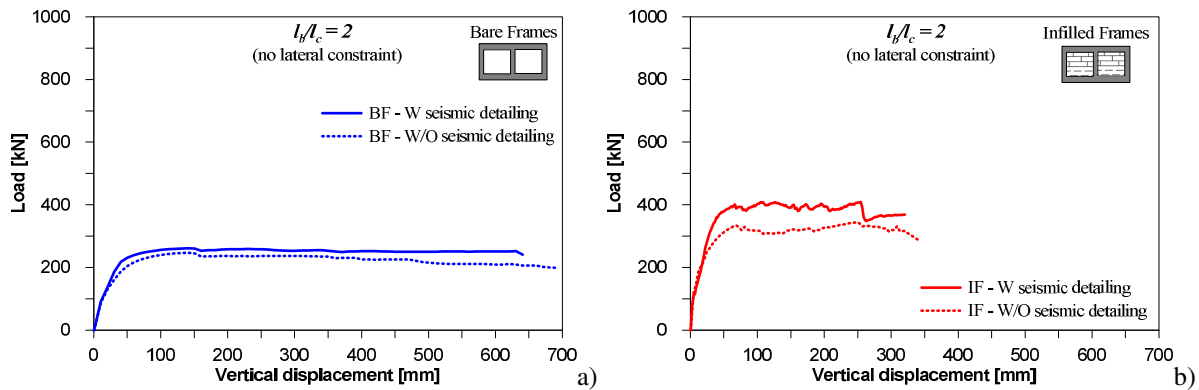

Figure 13: Pushdown curves of specimens with l_b/l_c=2 and no lateral constraints: a) bare frames with and without seismic detailing; b) infilled frames with and without seismic detailing.
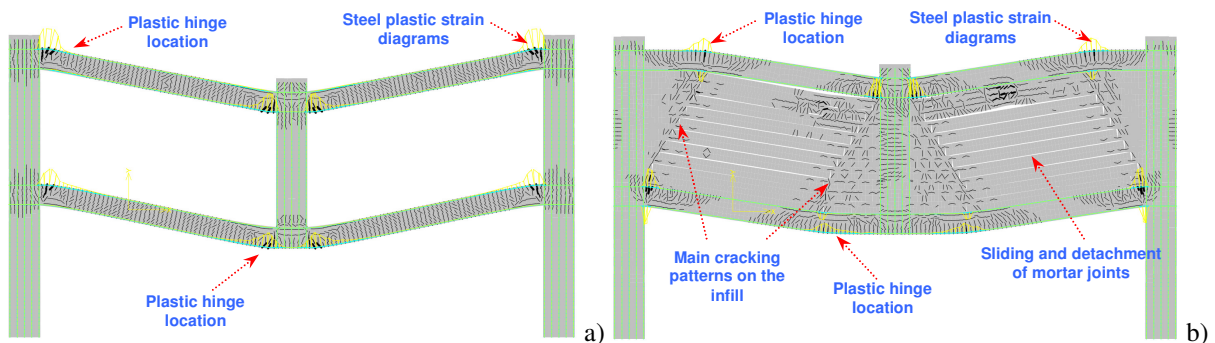

Figure 14: Cracking pattern recognized on the FE model at the end of the pushdown test of specimens with l_b/l_c=2 and rigid lateral constrains: a) bare frame; b) infilled frame.

4.3 Quantification of and capacity and demand modification due to infills

Fig. 15 shows the ratios between infilled frame and bare frame peak loads (P^*_{inf} and P^*_{bare}) under the different investigated conditions (aspect ratio, lateral constraint (LC), seismic detail-

ing (SD)). The aspect ratio of the frames plays the major role. In fact, square frames provide spread confinement on the masonry, which results in a major infill contribution to the overall strength due to the increased strength. This is much more evident for the frames not provided with seismic detailing and lateral constrains, where the modification of the overall capacity produces by the infills achieves +209%. For the frames having $l_b/l_c=2$ the influence of infills is less relevant but still significant. In this case the tests have highlight minor dependence of the strength increment with the lateral constraint and seismic detailing conditions, recording an average increment of +45%.

Dynamic load amplification factors (λ_d) obtained for the specimens are reported as bar charts in Fig. 16. Square bare frames and infilled frames have shown similar dynamic amplification factors, which stay in the range 3.5-4.7, apart from for the case of non-seismically designed frames without lateral constraint. The effect of masonry infills on the modification of λ_d was more relevant when $l_b/l_c=2$. In these cases the increase of dynamic load demands ranged between +30% and +60% depending on lateral constraint conditions, although he increment of dynamic load demand is however generally accompanied by an increase of bearing capacity. Capacity / demand ratios are finally shown in Fig. 17. The presence of infills resulted in a noticeable increase of β_s coefficients (Fig. 17a) especially for square specimens, where β_s was more than double with respect to bare frame cases. β_s coefficients of infilled frames with $l_b/l_c=1$ ranged between 7 and 10. On the contrary β_s coefficients assumed values between 1.28 and 2.0 for $l_b/l_c=2$.
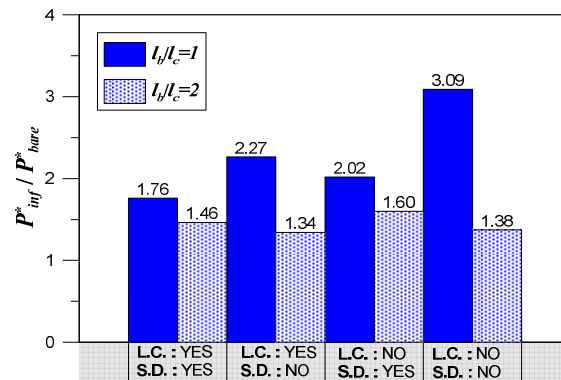

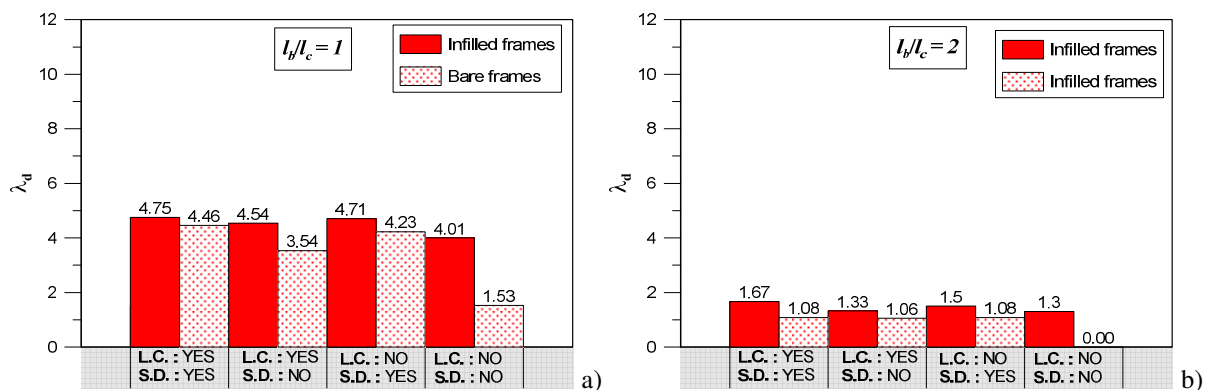Figure 15: Infilled frame / bare frame maximum strength ratios for the investigated conditions.

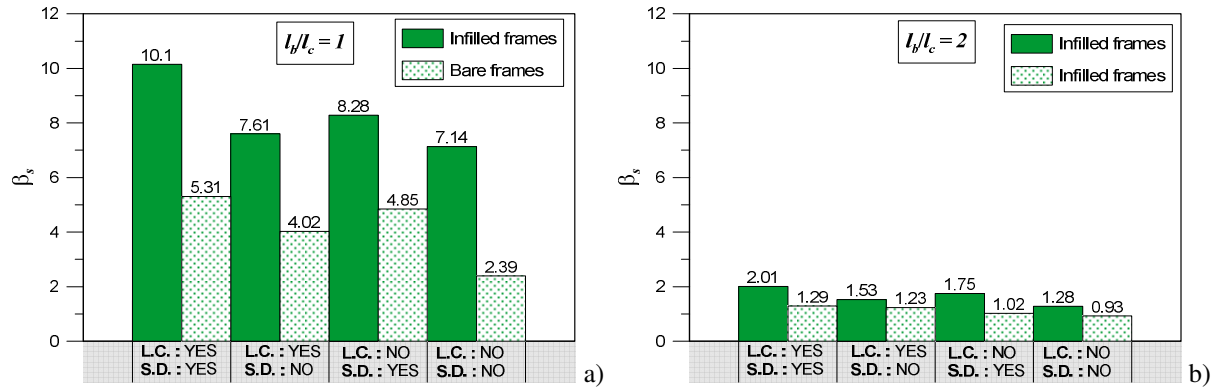Figure 16: Load amplification factors: a) $l_b/l_c=1$; b) $l_b/l_c=2$.

Figure 17: Capacity / demand ratios: a) $l_b/l_c=1$; b) $l_b/l_c=2$.

5 TESTING EQUIVALENT STRUT MODELLING APPROACH FOR THE SIMULATION OF PUSHDOWN RESPONSE OF INFILLED FRAMES

In order to find a computationally effective modelling strategy to simulate progressive collapse response, a possible adaption of equivalent strut modelling approach is here tested, while acknowledging that: a) load direction in case of column loss is vertical instead of horizontal; b) observed collapse mechanisms are different from those typical of infilled frames subjected to seismic actions. Numerical tests previously presented are reproduced with Open-Sees [38], using fiber-section approach to model beams and columns, and the equivalent strut model by Di Trapani et. al (2018) [37] to model infills. This model is based on a single concentric fiber-section strut (S1 strut) governed by a concrete-type stress-strain law. The definition of the equivalent strut properties follow the equation provided in [37]. This approach is tested in two possible configurations having different degree of complexity: 1-strut configuration (Fig. 18a) and 3-strut configuration (Fig. 18b). The 1-strut configuration is the original strut configuration of the model, where, for the determination of all the parameters, the length of the infill (l_b) is inverted with its height (h_c). In the 3-strut configuration, the same S1 strut is accompanied by two rigid struts (S2 struts) which start from the end of S1 strut and point toward top and bottom beams at a distance αl_b (Fig. 18b). S2 struts are included in the model to simulate in a more effective way the observed damage mechanism, in which, masonry at corners remains almost intact. The distance αl_b represents the position where the plastic hinge forms. From the damage patterns observed by the FE models pushdown tests it can be reasonably assumed that assumed αl_b=0.35 in the case in which l_b/h_c=1 and αl_b=0.1 if l_b/h_c=2.

The tests are carried out for four specimens among those previously tested, in detail these are seismically designed frames with and without lateral constraints and with square and rectangular aspect ratio (l_b/h_c=1 and l_b/h_c=2). Results of the comparisons are illustrated in Figs. 19 and 20. It can be observed that the prediction of the peak resistance results significantly improved in the case of 3-strut configuration. On the contrary 1-strut models generally show an understimation of the capacity. The better predictive capacity of 3-strut models is due to the effective identification of the reduced span length mechanism, which results in an increase of bearing capacity of the system. This can be also observed from the deformed shapes of the specimens reported in Figs. 21a and 21b, that highlight the consistency of 3-strut models deformed profiles with those recognized by the FE models.
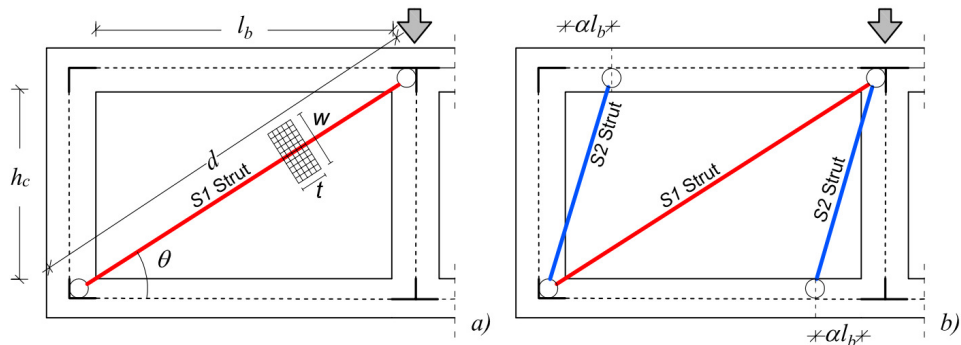
Figure 18: Possible equivalent strut configurations: a) 1-strut model; b) 3-strut model.
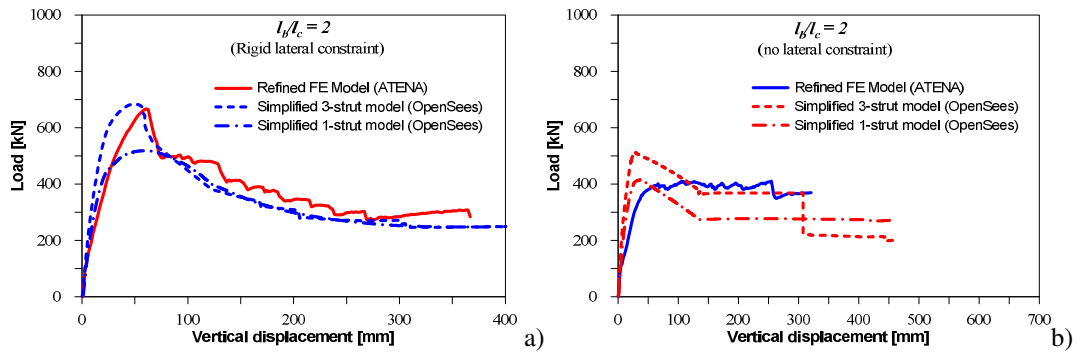

Figure 19: Possible equivalent strut configurations: a) 1-strut model; b) 3-strut model.

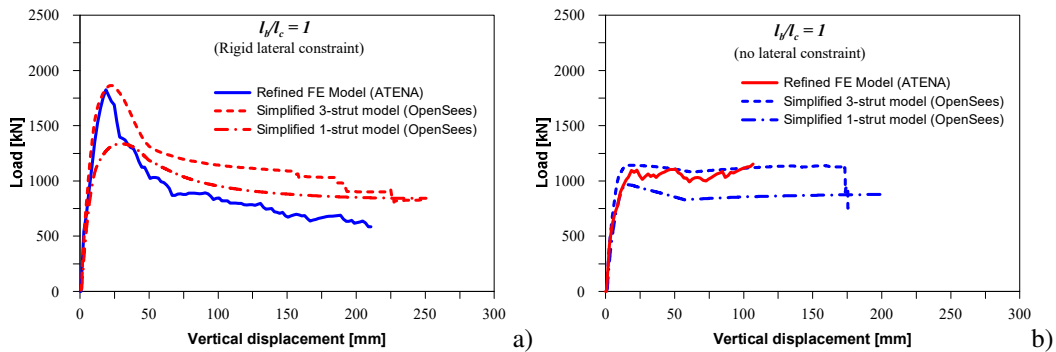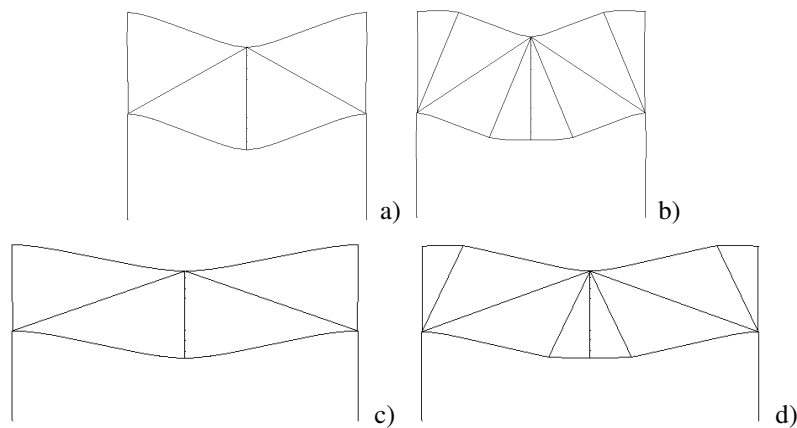Figure 20: Possible equivalent strut configurations: a) 1-strut model; b) 3-strut model.

Figure 21: Deformed shapes of 1-strut and 3-strut models of infilled frames with: a) 1-strut with rigid lateral constraints (l_b/h_c=1); b) 3-struts with rigid lateral constraints (l_b/h_c=1), c) 1-strut with rigid lateral constraints (l_b/h_c=2); d) 3-struts with rigid lateral constraints (l_b/h_c=2)

6 CONCLUSIONS

The paper has presented a numerical investigation regarding the influence of masonry infills on the progressive collapse response of reinforced concrete frame structures. Results have shown a primary role of infills on the response of the system to a perimetral column accidental loss scenario. The major findings can be summarized in the following points:

- In the progressive collapse mechanism infills work as diagonal struts providing additional resistance and at the same time modifying the internal forces distribution on frame members;
- Infills can increase the overall resistance in a significant way but their presence result in a inhibition of the potential activation of catenary mechanism, which instead is typical in the case of bare frames;
- Frame aspect ratio (l_b/l_c) is one of the most important parameters for both bare and infilled frames. Masonry infills in square specimens have much more influence on strength increment because of the major confinement action exerted by the frame;
- Lateral constrains degree is decisive on the collapse mode of bare and infilled frames. In fact, rigid constrains induce large axial force on beams which consequently have less deformation capacity. Then hence restrained frames are generally more resistant but show limited ductility and capacity to activate catenary mechanism;
- Equivalent strut macro-modelling seems a possible simple solution to effectively simulate progressive collapse, although further generalization of the tested approach is necessary.

REFERENCES

[1] B.A. Izzuddin, A.G. Vlassis, A.Y. Elghaz1ouli, D.A. Nethercot. Progressive collapse of multi-storey buildings due to sudden column loss—Part I: Simplified assessment framework. *Engineering Structures*, **30(5)**, 1308-1318, 2008.

[2] A.G. Vlassis, B.A Izzuddin, A.Y. Elghaz1ouli, D.A. Nethercot. Progressive collapse of multi-storey buildings due to sudden column loss — Part II: Application. *Engineering Structures*, **30(5)**, 1424-1438, 2008.

[3] P. Ren, Y. Li, X. Lu, H. Guan, Y. Zhou. Experimental investigation of progressive collapse resistance of one-way reinforced concrete beam–slab substructures under middle-column-removal scenario, *Engineering Structures* **118**, 28–40,2016.

[4] Y. Xiao, S. Kunnath, F.W. Li, Y.B. Zhao, H.S. Lew, Y. Bao. Collapse test of three-story half-scale reinforced concrete frame building. *ACI Structural Journal*, **112(4)**, 429-438, 2015.

[5] J. Yu, K.H. Tan, Experimental and numerical investigation on progressive collapse resistance of reinforced concrete beam column subassemblages. *Engineering Structures*, **55**, 90-106, 2013

[6] X.D. Pham, K.H. Tan, J. Yu. A simplified approach to assess progressive collapse resistance, *Engineering Structures*, **101**, 45-57, 2015

[7] A.T. Pham, K.H. Tan, J. Yu. Numerical investigations on static and dynamic r esponses of reinforced concrete sub-assemblages under progressive collapse. *Engineering Structures*, **149**, 2-20, 2017

[8] J. Weng, C.K. Lee, K.H. Tan, N.S. Lim. Damage as-sessment for reinforced concrete frames subject to progressive collapse, *Engineering Structures*, **149,** 147-160, 2017

[9] A.H. Arshian, G. Morgenthal. Three-dimensional progressive collapse analysis of reinforced concrete frame structures subjected to sequential column removal. *Engineering Structures*, **132**, 87–97, 2017

[10] A.B. Mehrabi, P.B.Shing, M.P. Schuller, L. Noland. Experimental Evaluation of Masonry-Infilled RC Frames, *J Struct Eng*, **122(3)**, 228-237, 1996.

[11] F. Colangelo. Pseudo-dynamic seismic response of reinforced concrete frames infilled with non-structural brick masonry, *Earthquake Eng Struct Dyn*, **34**, 1219–1241, 2005

[12] L. Cavaleri, F. Di Trapani. Cyclic response of masonry infilled RC frames: Experimental results and simplified modeling. *Soil Dynamics and Earthquake Engineering*, **65**, 224–242, 2014

[13] I. Caliò, B. Pantò. A macro-element modelling approach of Infilled Frame Structures, *Computers & Structures*, **143**,91–107, 2014.

[14] F. Di Trapani, M. Malavisi. Seismic fragility assessment of infilled frames subject to mainshock/aftershock sequences using a double incremental dynamic analysis approach. *Bulletin of Earthquake Engineering*, **17(1)**, 211-235, 2019.

[15] L. Cavaleri, F. Di Trapani. Prediction of the additional shear action on frame members due to infills, *Bulletin of Earthquake Engineering* **13(5)**,1425–1454, 2015.

[16] L. Cavaleri, F. Di Trapani, G. Macaluso, M. Papia. Reliability of code proposed models for assessment of masonry elastic moduli, *Ingegneria Sismica*, 29(1), 38–59, 2012.

[17] F. Di Trapani, P.B. Shing, L. Cavaleri. Macroelement Model for In-Plane and Out-of-Plane Responses of Masonry Infills in Frame Structures, *Journal of Structural Engineering*, **144(2)**, 04017198, 2018

[18] P.G. Asteris, L. Cavaleri, F. Di Trapani, F., V. Sarhosis. A macro-modelling approach for the analysis of infilled frame structures considering the effects of openings and vertical loads, *Structure and Infrastructure Engineering*, **12(5)**, 551-566, 2016.

[19] L. Cavaleri, F. Di Trapani, P.G. Asteris, V. Sarhosis. Influence of column shear failure on pushover based assessment of masonry infilled reinforced concrete framed structures: a case study, *Soil Dynamics and Earthquake Engineering*, **100**, 98–112, 2017.

[20] F.B. Xavier, L. Macorini, M.B. Izzuddin. Robustness of Multistory Buildings with Masonry Infill, *J Perform Constr Facil*, **29(5)**, B4014004, 2015.

[21] S. Farazman, B.A Izzuddin, D. Cormie. Influence of Unreinforced Masonry Infill Panels on the Robustness of Multistory Buildings, *J Perform Constr Facil*, **27(6)**, 673-6822013, 2013.

[22] K. Qian, B. Li. Effects of Masonry Infill Wall on the Performance of RC Frames to Resist Progressive Collapse, *J Struct Eng*, **143(9)**, 04017118, 2017

[23] S. Li, M.M. Kose, S. Shan, H. Sezen. Modeling Methods for Collapse Analysis of Reinforced Concrete Frames with Infill Walls, *J Struct Eng,* **154(4)**, 04019011, 2019.

[24] P. Castaldo, D. Gino, G. Bertagnoli, G. Mancini. Partial safety factor for resistance model uncertainties in 2D non-linear finite element analysis of reinforced concrete structures, *Engineering Structures*, **176**, 746-762, 2018.

[25] P. Castaldo, B. Palazzo, G. Alfano, M.F. Palumbo. Seismic reliability-based ductility demand for hardening and softening structures isolated by friction pendulum bearings, *Structural Control and Health Monitoring,* **25(11)**,e2256, 2018.

[26] P. Castaldo, M. De Iuliis. Effects of deep excavation on seismic vulnerability of existing reinforced concrete framed structures, *Soil Dynamics and Earthquake Engineering*, **64**, 102-112, 2014.

[27] P. Castaldo, D. Gino, V.I. Carbone, G. Mancini. Framework for definition of design formulations from empirical and semi-empirical resistance models, *Structural Concrete*, **19(4)**, 980-987, 2018.

[28] P. Castaldo, G. Mancini, B. Palazzo. Seismic reliability-based robustness assessment of three-dimensional reinforced concrete systems equipped with single-concave sliding devices, *Engineering Structures* **163**, 373-387, 2018.

[29] G. Campione, L. Cavaleri, F. Di Trapani, M.F. Ferrotto. Frictional effects in structural behavior of no end-connected steel-jacketed RC columns: experimental results and new approaches to model numerical and analytical response, *Journal of Structural Engineering*, **143(8)**, 04017070, 2017.

[30] G. Campione, L. Cavaleri, F. Di Trapani, G. Macaluso, G. Scaduto. Biaxial deformation and ductility domains for engineered rectangular RC cross-sections: a parametric study highlighting the positive roles of axial load, geometry and materials, *Engineering Structures*, **107(15)**, 116–134, 2016.

[31] L. Cavaleri, F. Di Trapani, P.G. Asteris, V. Sarhosis. Infuence of column shear failure on pushover based assessment of masonry infilled reinforced concrete framed structures: a case study, *Soil Dynamics and Earthquake Engineering*, **100**, 98–112, 2017.

[32] L. Cavaleri, F. Di Trapani, M.F. Ferrotto. A new hybrid procedure for the definition of seismic vulnerability in Mediterranean cross-border urban areas, *Natural Hazards*, **86**, 517-541, 2017

[33] L. Cavaleri, F. Di Trapani, M.F. Ferrotto, L. Davì. Stress-strain models for normal and high strength confined concrete: Test and comparison of literature models reliability in reproducing experimental results, *Ingegneria Sismica*, **34(3-4)**, 114-137, 2017.

[34] M.F. Ferrotto, O. Fischer, L. Cavaleri. A strategy for the finite element modeling of FRP-confined concrete columns subjected to preload, *Engineering Structures*, 173: 1054-1067, 2018.

[35] M.F. Ferrotto, O. Fischer, L. Cavaleri. Analysis-oriented stress–strain model of CRFP-confined circular concrete columns with applied preload, *Materials and Structures*, **51(2)**,44, 2018

[36] Cervenka Consulting, ATENA 2D v5. Prague, Czech Republic, 2014.

[37] F. Di Trapani, G. Bertagnoli, M.F. Ferrotto, D. Gino. Empirical equations for the direct defnition of stress-strain laws for fiber-section based macro-modeling of infilled frames. *Journal of Engineering Mechanics*, **144(11)**, 04018101, 2018.

[38] F. McKenna,. G.L. Fenves, M.H. Scott. Open system for earthquake engineering simulation, University of California, Berkeley, CA, 2000.